 Cytometry 31:217–228 (1998)

Analysis of Image Sequences in Fluorescence Videomicroscopy of Stationary Objects

Noël Bonnet[1,2]* **and Jean-Marie Zahm**[1]

[1]INSERM Unit 314 (IFR 53 Biomolecules), Reims, France
[2]LERI, University of Reims, Reims, France

Received 9 January 1997; Accepted 1 December 1997

Fluorescence videomicroscopy allows the temporal behavior of biological specimens to be studied at the cellular level. We describe two types of methods that can be used for extracting quantitative information from image sequences: the modeling approach, which is mainly local, and multivariate statistical analysis, which provides a global approach. The potentials for use of these two methods are illustrated through a simulation example and actual examples dealing with the study of chloride secretion by airway epithelial cells. We define some guidelines for making a choice between these two approaches, bearing in mind that a blend of these two methodologies is also possible. Cytometry 31: 217–228, 1998. © 1998 Wiley-Liss, Inc.

Key terms: videomicroscopy; fluorescence; image sequences; quantification; modeling; multivariate statistical analysis

Today the microscope can be viewed as a dynamic instrument allowing the study of biological activity of living cells in real time. Ionic concentrations inside cells change quickly and dramatically and underlie a wide range of cellular processes, including development, growth, secretion, and wound repair. Thus, it is important to observe and understand them.

Fluorescence videomicroscopy of ionic gradients allows one to record the evolution of such phenomena as function of time (18,32). Ionic changes may also occur differently in different cell phenotypes, rendering necessary the spatial analysis of these changes. The ability to interface videocameras and computer technology to the conventional microscope made it possible to derive quantitative data from image sequences of cells (6,19,31). This paper is limited to the study of stationary objects thus, the problem of tracking moving objects can be ignored. Therefore, in the following discussion, we assume that different digitally recorded images represent the evolution of fluorescent specimens as a function of time, and that these images are spatially registered. That is, that pixel number p in one image corresponds to the same location on the object as pixel number p in any image of the series. When the different images are not registered, automatic registration procedures (e.g., based on the cross-correlation coefficient or on mutual information) can be used.

In the large majority of papers dealing with time-resolved fluorescence microscopy, the analysis of data consists of displaying only the variation in fluorescence intensity, as a function of time, for several regions of interest (ROIs) selected by the experimentalist. We believe that a more efficient data analysis procedure can be used. The aim of this paper is thus to review the methodologies that can be followed in order to extract qualitative and quantitative information from such a series of images, in addition to visual inspection of the images as a gallery or as a movie. Although these methodologies are not novel, they have neither been used, nor compared, in the context of time-resolved fluorescence microscopy.

The various approaches that can be are discussed under Methods. From our point of view, there are mainly two approaches: the local approach, in which ROIs are analyzed independent of the others; and the global approach, in which the whole data set is analyzed at once. In the former case, what we can do is to model the evolution of the fluorescence intensity as a function of time. This modeling approach is sometimes called the ''parametric imaging'' method because, as a result of modeling the content of each pixel, we can build new images (the so-called parametric images) with the values(s) of the model parameter(s) obtained.

In the latter case, the whole data set of images is analyzed according to multivariate statistics. Multivariate

Contract grant sponsor: Association Française de Lutte contre la Mucoviscidose (AFLM; Artemis); Contract grant sponsor: Ministère de l'Enseignement Supérieur et de la Recherche (MESR); Contract grant number: 94.C.0137.

*Correspondence to: Noël Bonnet, INSERM Unit 314, 21, rue Clément Ader, 51685 Reims Cedex 2, France.
E-mail: noel.bonnet@univ-reims.fr

statistical analysis (MSA) has already been used in several fields of image processing: teledetection (26), nuclear medicine (10), magnetic resonance imaging (MRI) (14), electron microscopy (30), microanalysis (3,29). To the best of our knowledge, it has only been used once in the context of time-dependent fluorescence microscopy (20).

The possibilities and drawbacks of the different approaches are discussed under Results, first through a simulated example and then with an actual example dealing with the quantification of chloride secretions in cultured respiratory epithelial cells using a fluorescent probe. Until now, the functional activity of chloride channels in respiratory epithelial cells has been essentially assessed without taking into account the cell phenotype. The culture of airway epithelium explants provides an opportunity to obtain airway epithelial cells at different stages of differentiation (8), thereby allowing us to address the question of whether the efflux of chloride is dependent on a specific airway cell phenotype, with particular emphasis placed on the ciliated phenotype.

Finally, a discussion of the methods is presented, together with some guidelines for combining both approaches.

MATERIALS AND METHODS

This paper is mainly devoted to the description and comparison of methodologies for analyzing image sequences. Consequently, the experimental material provided is mainly intended to illustrate the procedures.

Experimental

Respiratory epithelial cells were cultured from explants of human nasal polyps. After 3 days in culture, outgrowths around the explants contained numerous ciliated cells and undifferentiated cells. The cultures were loaded with the chloride-sensitive indicator 6-methoxy-N-(sulfopropyl)-quinolinium (SPQ) (Molecular Probes, Eugene, OR) and placed on the heated stage (37°C) of an inverted microscope (Zeiss IM35; Zeiss, Oberkochem, Germany) and incubated in a chloride-depleted buffer in the presence or absence of 25 μM forskolin (Sigma, L'Isle d'Abeau, France) (34). During this incubation period, fluorescence videoimages were recorded every minute for 15 min, using a low-level SIT camera (Lhesa, Cergy-Pointoise, France) and a Sparc2 Sun workstation (Sun Microsystems, Mountain View, CA) equipped with a Parallax video board (Parallax Graphics, Santa Clara, CA).

Figure 1 shows four images (numbers n = 1, 5, 10, and 15) out of a series of 15 images recorded by fluorescence videomicroscopy. Figure 1A corresponds to images recorded from cells incubated in a chloride-depleted buffer in the absence of forskolin, whereas the images in Figure 1B were obtained from cells incubated with 25 μM forskolin in the chloride-depleted buffer. The aim of the study was to compare the temporal behavior of different populations of cells (e.g., ciliated and nonciliated) or of one particular cell phenotype as a function of different external conditions (stimulation of chloride secretion by the cAMP or Ca^{2+} pathway).

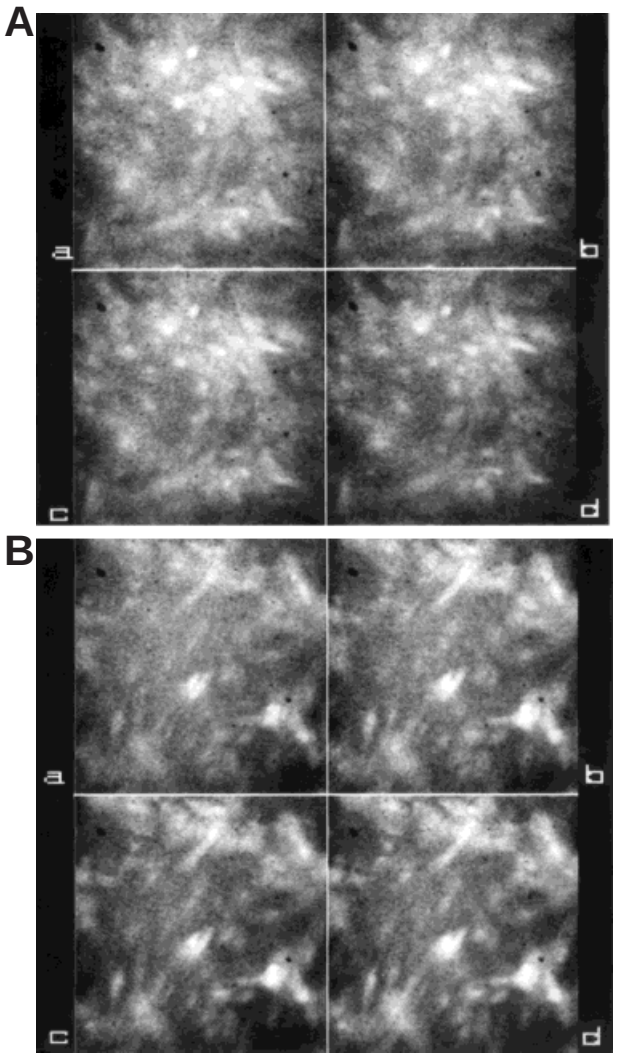

FIG. 1. **A:** Four of 15 images of a temporal sequence recorded every minute by fluorescence videomicroscopy. (Respiratory epithelial cells in culture, loaded with the SPQ probe used for the study of chloride secretion.) Images displayed are numbers 1, 5, 10, and 15 in the series. **B:** Four (of 15) images of a similar series following stimulation with forskolin.

Figure 2 shows images that correspond to the same experimental protocol. However, in that specific sequence, some cells, located at the periphery of the outgrowth, move during the image acquisition. In that situation, we will see that the cell movement precludes an automatic study of the time fluorescence variation.

Simulation

In order to convince the reader that, on the proviso that objects are not moving, complicated situations can be handled by the procedures described in this paper, we have built an artificial image sequence to help illustrate some of the more advanced capabilities of these procedures (It should be stressed that the purpose of the simulation is not to reproduce the experimental situation. Its only aim is to illustrate the capabilities and the limitations of the different methods, in a well-controlled situation, where the expected output is known).

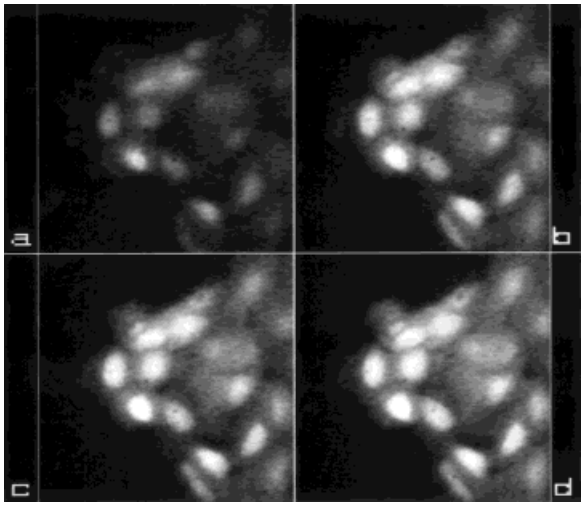

FIG. 2. Four images out of a sequence of 19 images similar to those of Figure 1. The difference is that some of the cells are moving, which makes the automatic analysis more difficult.

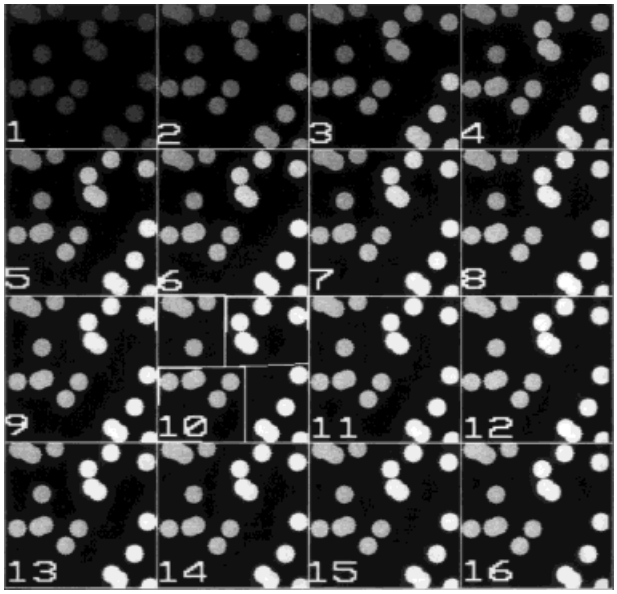

FIG. 3. Simulated image series. The background intensity is set constant; the initial fluorescence intensity is the same for all cells. Four groups of cells (top left, top right, bottom left, bottom right) are simulated. Their temporal behavior differs by **(a)** the overall intensity increase (left versus right), and **(b)** the speed of increase (top versus bottom).

The sequence (of 16 images, 128×128 pixels each) was constructed as follows: the area under investigation was composed of five regions, with five different temporal behaviors. The background intensity was set to a constant level. The temporal behavior of fluorescent objects (''cells'') was simulated according to the three-parameter model:

$$I_t = A + B \cdot (1 - e^{-C \cdot t})$$

where t stands for time. For all ''cells,'' the initial fluorescence intensity was set to A = 30. Cells in the left part of the field corresponded to B = 80, while cells in the right part corresponded to B = 150. Cells in the top part of the field corresponded to C = 0.2, while cells in the bottom part corresponded to C = 0.4. Thus, we had four groups of cells, representing four phenotypes, with different temporal behavior. Poisson noise was added to the simulated images. The sixteen images of the sequence are displayed in Figure 3.

Methods for Analyzing Image Sequences

The different images of the series will be denoted as $I_t(i,j)$, where (i,j) denotes an image pixel (p = 1 . . . P) and t denotes the image number (t = 1 . . . N), which is equivalent to time. (Note that all the procedures described below can be extended to work in three dimensions instead of two dimensions, but we will restrict our discussion to conventional two-dimensional microscopy.) The question we want to address is how to display and quantify the useful information contained in the data set. One thing we have to perform first is the extraction of this useful information. It is necessary because image sequences contain much redundant information that obscures the useful information (mainly the intensity changes). For instance, displaying the image series as a gallery may be totally insufficient for a complete perception of the occurring phenomena. Displaying the sequence as a movie is much more efficient but may still be insufficient for comparing two different sequences. Furthermore, it does not permit quantitative measurement of the studied phenomena. Therefore, digital analysis of the image series is often necessary (17).

We believe that most of the methods that have been empirically devised for extracting information from large data sets fall within two main categories: modeling and parametric imaging on one side and MSA on the other side.

Modeling and parametric imaging. Since the basic entity in images is the pixel, one can first think to extract information from the evolution of this minimal unit as a function of time. [Note that a set of spatially equivalent pixels as a function of an external variable such as time, wavelength, and energy, is sometimes called a *dixel* (23) or a *texel*, but we will maintain the term *pixel* throughout this paper.] This evolution can be described either by a statistical parameter or by an analytical function of this variable. In both cases, one can speak of an evolution model. The identification of the model $M(\alpha)$ and the computation of its parameter(s) α constitute the modeling approach (16,24,27). Depending on the nature of the model, the identification of the model parameter(s) can be made according to statistical analysis, to linear programming (9), the least-squares method, for instance, or to nonlinear programming (12,16), such as the Simplex method for instance. Examples of different possibilities are given under the heading ''Which Models for the Modeling Approach?''

Since this approach has to be followed for each pixel of the images independently, we end up with a set of parameters $\alpha(i,j)$, from which we can build as many images as there are parameters. This procedure is illustrated in Figure 4. The synthesized images are called

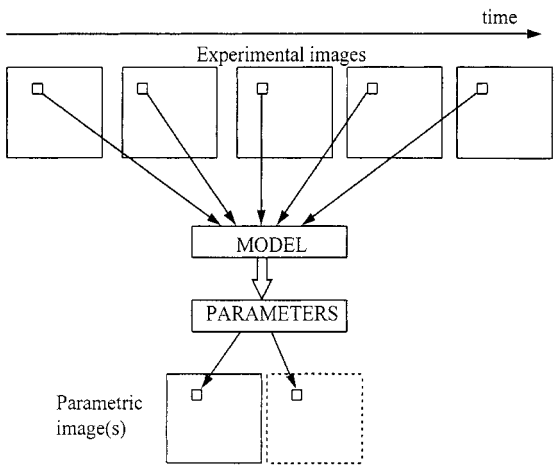

FIG. 4. Schematic illustration of the modeling approach. For each pixel of the image series, the intensity variation (as a function of time) is compared to a predetermined model. The comparison provides the value(s) of the model parameter(s). This value is used to synthesize a new image, the parametric image, which concentrates the information contained in the whole original series. For multi-parameters models, several parametric images can be built.

parametric images because the digital values that constitute them are proportional to the parameters of the model assumed to describe the temporal evolution, computed locally.

Philosophy of the method. The aim of the method is to concentrate the information contained in a large (at least 3, but possibly 10s) number of images into a small (generally ≤ 3) number of parametric images. The visualization of these images is assumed to be more convenient than the visualization of the original image series, because only the varying information has been retained and the redundant information has been discarded. Furthermore, the information contained in these images is directly quantitative, as they are built from the values of quantitative parameters. Whether this quantitative information can be used for interpreting the results of the experiment depends on the choice of the model (pertinent or not).

Drawbacks of the method. Several drawbacks of the method may be identified. The first drawbacks are of a technical nature: since the model is identified on a pixel basis, the statistical significance of the estimated parameters is questionable. If the experimental images are slightly noisy, the uncertainty in the modeling can be very high and the parametric images themselves are noisy.

The other drawbacks are related more to the philosophy of the method, which relies on the preexistence of an a priori model. Since many different models can be presupposed, the question arises as to ''how robust are the results and the conclusions to a change in the assumed model?''

A variant of the method. Instead of applying the modeling approach at the pixel level (which raises the question of the statistical significance), it is possible to apply it at the level of an ROI. These ROIs are constituted of basic objects, consisting of cells, nuclei, biological compartments, and so forth. The first problem is thus to define these ROIs. This can be attempted by automatic methods (image segmentation) or, in more difficult situations, can be done interactively. Then, fluorescence signal intensities are averaged spatially within the ROI and the modeling is performed with the averaged intensities. In this case, no parametric imaging is performed.

Multivariate statistical analysis. At the opposite of the local modeling approach, a global approach was devised by the statisticians at the beginning of the twentieth, in order to analyze a data set as a whole. This approach, which consider data sets as matrices (the variables versus the individuals), tries to approximate a complex set as a linear combination of simpler sets. When efficient computers became available, this method has been extended to image series, where the pixels play the role of individuals and the image numbers (i.e., time in temporal series) play the role of variables. For a data set composed of 10 images (512×512 pixels) for instance, the initial matrix to process is a $262{,}144 \times 10$ matrix. The mathematical procedure to use for processing this matrix is given in many textbooks (1,22) and only a brief description of the different steps will be given here. The first consists of computing the covariance (or correlation) matrix of the initial matrix X:

$$Y = X^t \cdot X. \tag{1}$$

This small matrix (10×10 in our sample case) concentrates the main information into image variances (along the diagonal of Y) and into image covariances (off the diagonal of Y). Several variants of this preliminary computation (centering the data or not; performing pixel and/or image normalization or not) lead to different variants of MSA, including principal components analysis, PCA; Karhunen-Loëve analysis, KL; and correspondence analysis, CA.

Then, what one tries to do is to define a new basis for the description of the data set (the initial basis is the R^N space, where N is the number of images). It was shown (1) that a useful new space ($R^{N'}$, $N' < N$) is the space spanned by the first N' eigenvectors of the variance-covariance matrix, associated with the highest eigenvalues. This is, in fact, equivalent to finding in the R^N space the directions of highest variance (see Fig. 5 for an illustration in two dimensions). Once these new basis vectors, also called orthogonal factorial axes, are defined, one can compute the coordinates of pixels and of images on them. The coordinates of each image of the series on the different factorial axes can be displayed. Usually, the images coordinates on two factorial axes (e.g., 1 and 2, 1 and 3, 2 and 3) are displayed simultaneously (two-dimensional plot), which generally allows to interpret the temporal behavior of the series (see Fig. 12, for instance). The coordinates of the pixels on the factorial axes can also be computed and displayed as factorial images (see figures 7, 11 and 13, for instance). It is thus possible to visualize which pixels contribute (positively or negatively) to the different facto-

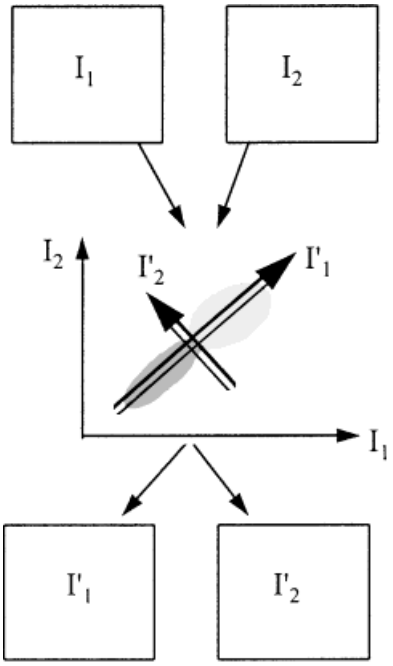

FIG. 5. Schematic illustration of the MSA approach. For a sequence composed of only two images, the content of one image can be represented as a function of the content of the other one. Pixels with similar properties (i.e., with similar couples of values) form clusters in the two-dimensional data space. The analysis consists in searching for the direction of maximum variance (I'_1). When the sequence is composed of more than two images, the process can be generalized in a N-dimensional data space. The next step after the main axis (I'_1) is found consists in searching for the direction of the maximum residual variance (axis I'_2), and so on. When the significant directions are found, the coordinates of pixels on these new axes can be used to build $N' < N$ new images (the so-called factorial images), which also concentrate the information contained in the original sequence.

rial axes. This second visualization mode helps complement the interpretation of the data set.

Philosophy of the method. The aim of the method is also to concentrate the information from a large number (N) of experimental images into a smaller number (N′) of images (the orthogonal factorial images).

These images are assumed to be more easily interpretable, as each carries a different ''source of information.'' There are two main differences with the previous approach.

1. It is not necessary to provide a model at the beginning of the analysis. The models for the evolution of the different sources of information (factorial images) as a function of the external variable (time) are provided by the analysis itself (not in analytic form, but as the weights of the different images onto the new orthogonal basis).

2. The whole data set is analyzed simultaneously. This makes the analysis more robust. Noise, for instance, is often rejected into high-order (i.e., with the smallest eigenvalues) factorial components, so that the most important (low-order) components are often free of noise.

Drawbacks of the method. The counterparts of the advantages described above are as follows:

1. The method cannot be directly quantitative. The reason is that the original data set is decomposed into a linear combination of orthogonal components. But there is no specific reason that the ''true'' underlying components are orthogonal. Assume that an image series can be described by two distributions:

$$I_t(i,j) = a_t\, A(i,j) + b_t\, B(i,j)$$

where a_t and b_t are two underlying models. The series can be decomposed into:

$$I_t(i,j) = \sum_{k=1}^{N} c_{k,t} C_k(i,j) \qquad (2)$$

where $\langle C_k, C_{k'} \rangle = 0$ for $k' \neq k$ and $C_k(i,j)$ are the factorial images.

We will find that the number of significant components (the question of the determination of the number of components is not specifically addressed in this paper but was studied in a number of papers, found in the references cited in ref 4) is two, but there is no reason to identify $c_{1,t}$ to a_t, nor $c_{2,t}$ to b_t. Therefore, the pixel weights $C_k(i,j)$ cannot be identified with the ''true'' weights A(i,j) and B(i,j), and no quantitative conclusions can be drawn. The only thing we can anticipate (and which is verified in practice) is that if A(i,j) is of greater variance than B(i,j), $C_1(i,j)$ is ''close'' to A(i,j) and $C_2(i,j)$ is ''close'' to B(i,j). The closeness depends on the covariance between A and B. A number of methods have been suggested for moving from the first step (abstract analysis) of MSA to the second step, where the factorial axes are rotated to form an oblique basis as close as possible to the underlying models (11,25).

2. When a model is valid only for a small number of pixels, it can be obscured (or completely hidden) by models valid for the majority of pixels.

Which Models for the Modeling Approach?

In the previous paragraph, we have discussed the possibility to model the content of any pixel, and to synthesize parametric images, without entering the details of the modeling step. We classify the possibilities into three categories: statistically based models, analytical models, and reference models.

Statistically based models. Each pixel (i,j) is described by a set of intensity values I_t, where t stands for time (or, equivalently, image number). Thus, many statistical parameters can be extracted from this set of values. In some situations, these parameters can be sufficient to characterize the temporal evolution and to extract the useful information.

Examples of such parameters:

the absolute difference: $D = I_{max} - I_{min}$

where I_{max} and I_{min} are the maximum values of the pixel as a function of time, respectively

the relative difference: $RD = D/I_M$

where I_M is the mean intensity value of the pixel.

the standard deviation: σ; pixels whose intensity vary more than others will be depicted (as bright spots) in the parametric image

the relative standard deviation, or coefficient of variation:

$$CV = \sigma/I_M.$$

Relative variations (instead of absolute variations) will be enhanced

the sum of the absolute value of the differences (SAVD):

$$SAVD = \sum_{t=2}^{N} |I_t - I_{t-1}| \quad (3)$$

the relative SAVD: $RSAVD = SAVD/I_M$ (4)

Analytical models. Rather often, the physical basis of the studied phenomena can help to give an idea of the expected temporal evolution. This knowledge can be put in the form of an analytical model, where the intensity variation is expressed as a function of time (or image number n) and of a parameter vector α:

$$I_t = f(t, \alpha). \quad (5)$$

In this case, the modeling strategy consists of estimating the parameter vector α from the experimental values

$$\alpha = g(I_t). \quad (6)$$

Depending on the nature of the model f, this estimation g can be made by linear programming, nonlinear programming, or stochastic methods (simulated annealing, ref. 21; genetic algorithms, ref. 13).

A nonexhaustive list of analytical models includes:

the linear model:

$$I_t = \alpha(0) + \alpha(1) \cdot t, \text{ with 2 parameters} \quad (7)$$

the Mth-order polynomial model:

$$I_t = \sum_{m=0}^{M} \alpha(m) \cdot t^m, \text{ with } (M+1) \text{ parameters} \quad (8)$$

the γ function:

$$I_t = \alpha(0) \cdot t\,\alpha(1) \exp(-\alpha(2) \cdot t), \text{ with 3 parameters,} \quad (9)$$

the β function:

$$I_t = \alpha(0) \cdot t^{\alpha(1)} (k - t)^{\alpha(2)}), \text{ with 3 parameters,} \quad (10)$$

the power law model:

$$I_t = \alpha(0) \cdot t^{\alpha(1)}, \text{ with 2 parameters, a special case of the two previous more general functions} \quad (11)$$

the monosinusoidal model:

$$I_t = \alpha(0) \sin [\alpha(1) \cdot t + \alpha(2)], \text{ with 3 parameters} \quad (12)$$

Reference models. In addition to modeling the data according to their statistical content or to an analytical model, it is also possible to do it with reference to one or several ''external'' models, i.e., to sets of intensity values (corresponding to the same time sets) to which the experimental data set is compared. Within this category, probably the best known approach is the least-squares fitting technique. But some other techniques are also available that are less demanding in terms of a priori knowledge.

Least-squares fitting technique. Here we assume that the experimental data are a linear combination of models that are known by advance (e.g., after measurements made on ''pure'' specimens):

$$I_t = \sum_{m=1}^{M} \alpha(m) \cdot A_{mt} \quad (13)$$

where A_{mt} is the tth value of the model A_m.

In this case, the modeling consists in evaluating locally the weighting coefficients α, thus producing the M parametric images $\alpha(i,j)$. Techniques for performing least-squares fitting are described in textbooks (2).

Correlation technique. Sometimes, the data set is still a linear combination of several models, but only one (A_0) is known. In this situation, the best one has to do is to compute the correlation coefficient between the experimental set I and the known model A_0:

$$\rho = \frac{E[I_t \cdot A_0] - E[I_t] \cdot E[A_0]}{\sigma_{It} \cdot \alpha_{A0}}. \quad (14)$$

The parametric image $\rho(i,j)$ displays parts of the image sequence that are correlated with the model A_0 and those that are not.

Alternatively, the angle between the two vectors:

$$(I_t, A_0) = \text{Acos} [<I_t, A_0>/(|I_t| \cdot |A_0|)] \quad (15)$$

where $<,>$ stands for the scalar product and $|\cdot|$ for the vector norm, can also be used as a measure of resemblance.

An intermediate situation (between the situation where only one model in known and the situation where all the underlying models are known) is the following. Assume

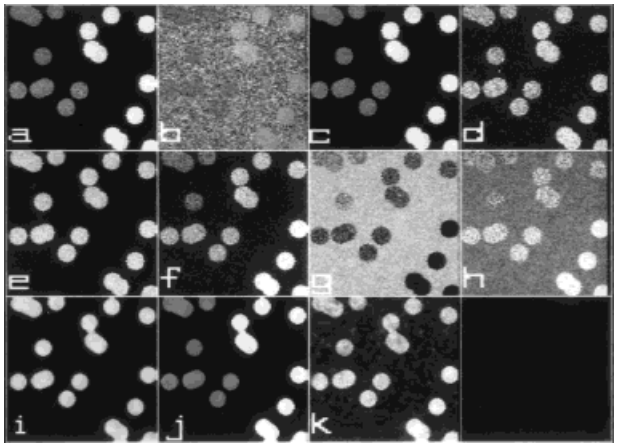

FIG. 6. Modeling analysis of the simulated image sequence (Fig. 3). **a–d:** Parametric image of the statistical parameters (Max − Min), (Max − Min)/Mean, σ, and SAVD. **e–h:** Parametric images of the four parameters [α(m), m = 0 to 3] of a third-order polynomial model. **i–k:** Parametric images of the three parameters (A, B, and C) of the model: $I(t) = A + B \cdot (1 - e^{-C \cdot t})$ These three images can be used for interpreting the image series. All cells are characterized by the same initial fluorescence intensity (parameter A, i); cells in the left and right parts differ by the overall fluorescence increase (parameter B, j); cells in the top and bottom parts differ by the speed of the fluorescence increase (parameter C, k).

the experimental series is the superimposition of (at least) two models: the ''useful'' model A_0, which is the object of the study, and an ''unuseful'' model A_1 (e.g., due to the presence of an unavoidable fluorescent species), which disturbs the study. The question arises as ''how to reject most of the unuseful contribution while keeping the maximum of the useful contribution?'' For this, we have to project the original data (represented by the vector I_n) onto an optimal vector (e) defined as:

$$e = A_0 - \frac{<A_0 \cdot A_1>}{<A_1 \cdot A_1>} A_1 \qquad (16)$$

so that $<e \cdot A_1> = 0$ (28,33).

In summary, many models are available for applying the modeling technique. No general rule can be given for choosing among them. When the physical basis of the experimental process is known, it is certainly better to choose the corresponding analytical model or a reference model procedure. But when no such model is available, one must rely on a statistical model.

RESULTS

Simulation

Several examples of parametric images obtained from the simulated image sequence displayed in Figure 3 are shown in Figure 6. Figure 6a,b is the parametric image corresponding to the statistical parameters (max − min) and (max − min)/mean. Figure 6c,d displays the parametric images of the standard deviation (σ) and the sum of the absolute value of the differences (SAVD). Clearly, the problem at hand is too complicated (with four different types of cells) for a simple interpretation only based on these simple parametric images. Figure 6e–h shows results of parametric imaging according to a third-order polynomial model:

$$I_t = \sum_{m=0}^{3} \alpha(m) \cdot t^m.$$

The different parametric images display the parameters α(m), for m = 0 to 3, obtained for each pixel. Although some properties of the different groups of cells can be inferred from these parametric images, the interpretation is made difficult, because the model used for modeling was not the underlying (true) model. Figure 6i–k displays the parameters of the model

$$I_t = A + B \cdot (1 - e^{-C \cdot t}) \qquad (17)$$

which was the model used for the simulation. In that case, the parametric images can be used directly for the interpretation. The first parametric image corresponds to the initial (t = 0) fluorescence intensity: it is the same for all cells in this case. The second parametric image corresponds to the total variation of fluorescence intensity (parameter B); it permits distinction of two groups of cells (left and right parts of the field). The third parametric image corresponds to the rate of intensity variation (parameter C): it also permits distinction of two groups of cells (top and bottom parts). Altogether, four groups of cells can be recognized. But this has only been made possible because the underlying model was known.

The factorial images corresponding to the first four eigenvalues are displayed in Figure 7a–d. Note that besides the ''trivial'' factorial image (Fig. 7a) representing the average value of the pixel intensities, only two factorial images (Fig. 7b,c) contain structural information. This can be explained by the fact that there are only two sources of information. The first source of information is explained by the factorial axis number 1: it opposes cells in the left part to cells in the right part. A careful look at the temporal behavior of these cells tells us that the meaning of this source of information is the amplitude of intensity variation (parameter B). The second source of information is carried by the factorial axis number 2. It opposes cells in the top region to cells in the bottom region. It represents the speed of fluorescence intensity increase. The weights (scores) of the 16 original images on the factorial axes 1 and 2 are displayed in graphical form in Figure 7e. The data set can be interpreted on the basis of Figure 7a–c and 7e.

From these factorial images, the number of classes (i.e., groups of pixels with similar temporal behavior) can be estimated, without reference to any model. Figure 7f displays the scatterplot (or two-dimensional histogram: the content of one image versus the content of another one) built from the two factorial images (Fig. 7b,c). Here, we obtain five clusters, which correspond to the five different regions, i.e., the five different temporal behaviors. Automatic clustering (5,15) allows to obtain the localization of these different regions: the result of an

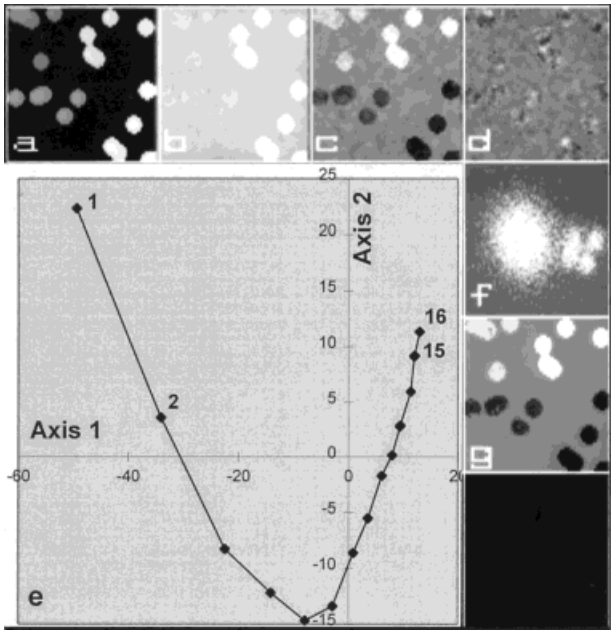

FIG. 7. Multivariate statistical analysis of the simulated image series (Fig. 3). **a–d:** The first four factorial images. a: The first (trivial) image is simply the average of the eight original images. b: First ''true'' factorial image: cells in the left part are opposed to cells in the right part. This is the main source of information (displayed as black/white contrast) differentiating the different underlying models. c: Second factorial image: here, the main opposition is between cells in the top part and cells in the bottom part. This is the second source of information. d: Mainly noise, and no structural information. **e:** Display of the scores of the different images on the factorial axes 1 (horizontal) and 2 (vertical). **f:** Scatterplot (or two-dimensional histogram) corresponding to the two factorial images (b,c). Here, the five clusters correspond to the five different regions present in the original data set. **g:** By automatic clustering, the five regions can be obtained. The gray levels represent the index of classification of the pixels into five classes (four classes of cells and background), after automatic classification.

automatic classification procedure is displayed in Figure 7g (the four groups of cells, and the background, are labelled differently).

Experimental Situation

The temporal fluorescence variations measured in regions of interest located on either ciliated or nonciliated cells are shown in Figure 8, expressed as a percentage of the initial fluorescence in each cell. In control situations, without forskolin stimulation (Fig. 8A), we observed a progressive increase in fluorescence that reached a plateau value within 5 min. The fluorescence increase measured in ciliated cells was significantly higher (+17%, $P < 0.001$) than the fluorescence increase measured in nonciliated cells (+7%). After forskolin stimulation (Fig. 8B), the fluorescence increase observed in both nonciliated cells and ciliated cells was significantly higher (+18% and +36%, respectively, $P < 0.001$) than that observed in the absence of forskolin stimulation. Furthermore, forskolin stimulation induced a significantly higher fluorescence increase in ciliated cells compared with nonciliated cells. The increase in SPQ fluorescence, representative of a decrease in intracellular chloride concentration, demonstrated that well-differentiated airway cells such as ciliated cells had a higher cAMP-dependent activation of chloride conductance compared with nonciliated cells.

The modeling process can be performed for a single pixel or for a group of pixels (also called ROI). When each pixel is modeled in turn, parametric images can be produced. Figure 9A,B shows examples of statistical parametric images computed for the control series (Fig. 9A) and the forskolin series (Fig. 9B). The absolute standard deviation (a) and the relative standard deviation (b) were used as statistical parameters. Figure 10a–c presents the images of the parameters A, B, and C, respectively, for the three-parameter model described above. Figure 10d displays the χ^2 values, that measure the quality of the modeling for each pixel. This was done for the control series (Fig. 10A) and for the forskolin series (Fig. 10B).

All parametric images (and many others that can be constructed) concentrate and display a part of the useful information. The main problem is to choose which parametric image(s) is really representative of the information of interest (or, in other words, which model must be applied). As stated above, a variant of this procedure consists of considering regions of interest (here, cells) instead of single pixels. As a result of the averaging process, statistics become improved but, on the other hand, displaying the results as images is no longer feasible.

One way to avoid having to choose a model is to perform MSA. Figures 11 and 12 display the results of a principal component analysis (PCA), which is one of the variants of MSA available. Figure 11 displays the first four factorial images, with Figure 11a showing the so-called ''trivial'' factorial image, which represents the average of the whole series. The other factorial images (Fig. 11b–d) represent 11%, 8%, and 7% of the total variance, respectively, for the control series (Fig. 11A) and 18%, 9%, and 7% for the forskolin series (Fig. 11B). Figure 12 shows the weighting of the different images of the experimental sequence on the first factorial axis, which represents most of the useful information (axis 2 represents second-order variations together with experimental artifacts such as dust on the camera lens; axis 3 contains mainly noise). Altogether, these two types of representation permit interpretation of the temporal behavior of the different classes of pixels, with an increase in the fluorescence signal as a function of time and a spatial differentiation according to the cell phenotypes. The ciliated cells, which were easily identified due to the beating of their cilia, exhibited the highest fluorescence variation, even in nonstimulated conditions.

In this experimental situation, the interpretation was fairly easy: the temporal evolution was globally monotonous, with an increase in the fluorescence signal as a function of time and spatial differentiation (Fig. 11b). One can see that the fluorescence increase is proportional to the initial fluorescence signal (nuclei that displayed a strong fluorescence also displayed a large fluorescence increase). This was confirmed by parametric images displaying the relative standard deviation or the relative SAVD (not shown). Of course, our interest was not to interpret just one image series, but to compare different image sequences, corresponding to different situations (several

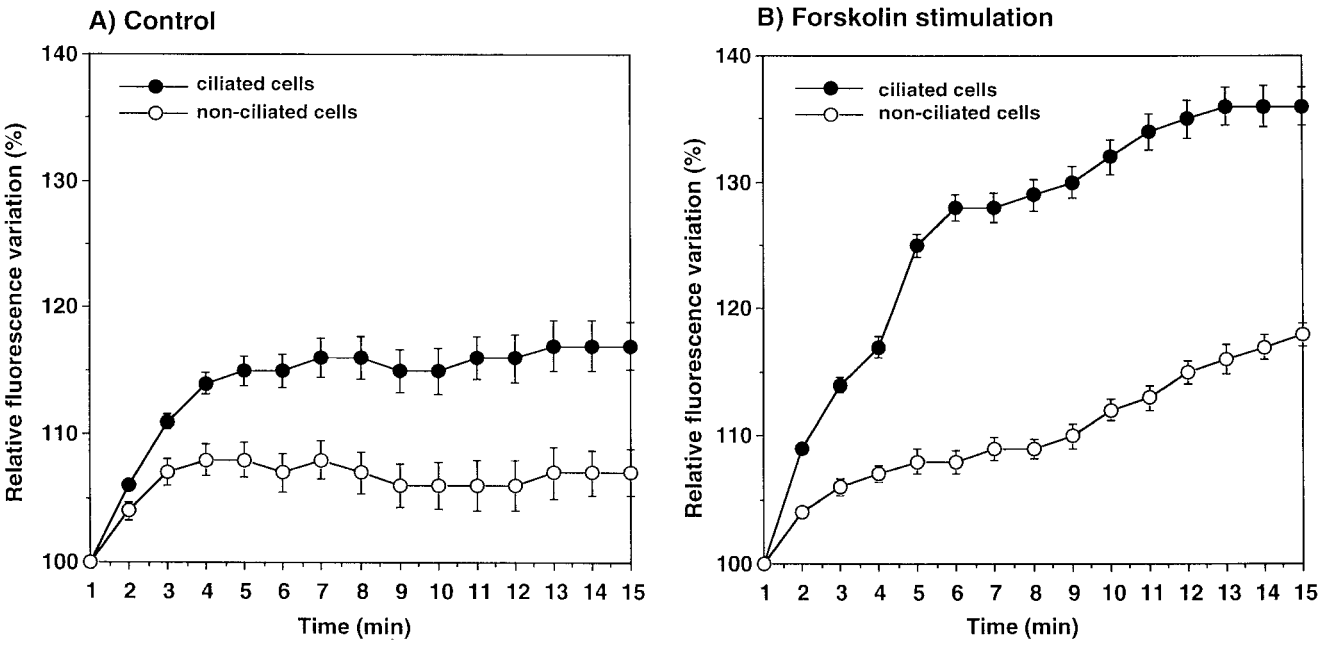

FIG. 8. Temporal fluorescence variations in regions of interest located on nonciliated cells and ciliated cells incubated or not with 25 μM forskolin. The fluorescence variations are expressed as the percentage of the initial fluorescence in each cell. Each point represents the mean ± S.E. of 30–40 different cells. The differences in fluorescence variations were tested using the Student's *t*-test.

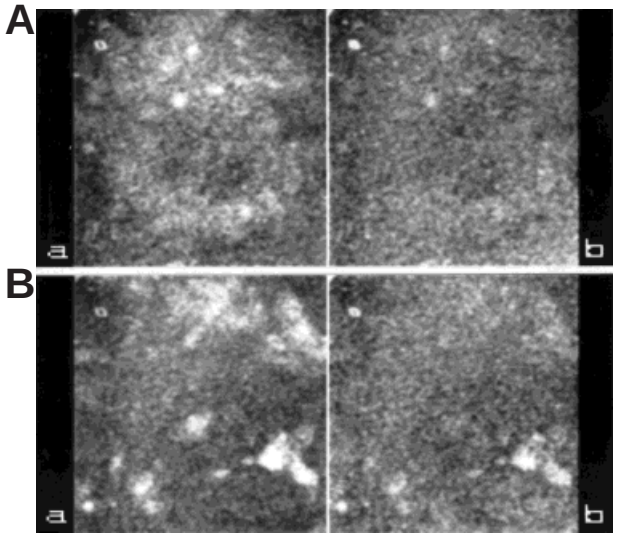

FIG. 9. Examples of statistical parametric images obtained from the experimental image series (Fig. 1). a: Standard deviation. b: Sum of the absolute values of the differences (SAVD). **A:** Results computed from Figure 1A. **B:** Results computed from Figure 1B.

''factorial curves'' analogous to the curve in figure 4 were superimposed). The interpretation of such curves and their usefulness for studying the chloride secretion capacity of respiratory epithelial cells will be reported in a companion paper (Zahm et al., in preparation).

Another Experimental Situation

From the fluorescence image sequence partly displayed in Figure 2, we obtain the four factorial images displayed in Figure 13. Figure 13a is the trivial factorial image (average of the series). The first factorial image (Fig. 13b) is dominated by the moving cells (arrowed). The black and white contrast on the two opposite sides of an object is characteristic of a small object displacement. This type of artifact in the factorial images is accompanied by ''false'' factorial curves (not shown).

DISCUSSION AND CONCLUSION

The availability of optical probes for biological activity associated with powerful image acquisition and analysis technology is becoming of major importance in the study of physiological parameters in living cells. Furthermore, the development of culture techniques now allows for the in vitro production of a diverse range of cell phenotypes within a cell population that were previously only encountered in vivo. It is obvious that different phenotypes within a cell population manifest different physiological behaviors. The main result of the experimental data analyzed in the present work (in order to illustrate the methodology described) concerns differences in chloride efflux observed in ciliated and in non-ciliated cells. It is noteworthy that this difference was observed even in the absence of any stimulation of the cAMP pathway, i.e., as occurs when cells are exposed to a hypotonic medium. The activation of a conductance pathway for chloride originates from the initial cell swelling induced by an hypotonic environment. The propensity for ciliated cells to be stimulated by the cAMP pathway as compared with nonciliated cells is related to the expression of the cystic fibrosis transmembrane regulator (CFTR) protein, which is exclusively located at the apical membrane domain of well-differenti-

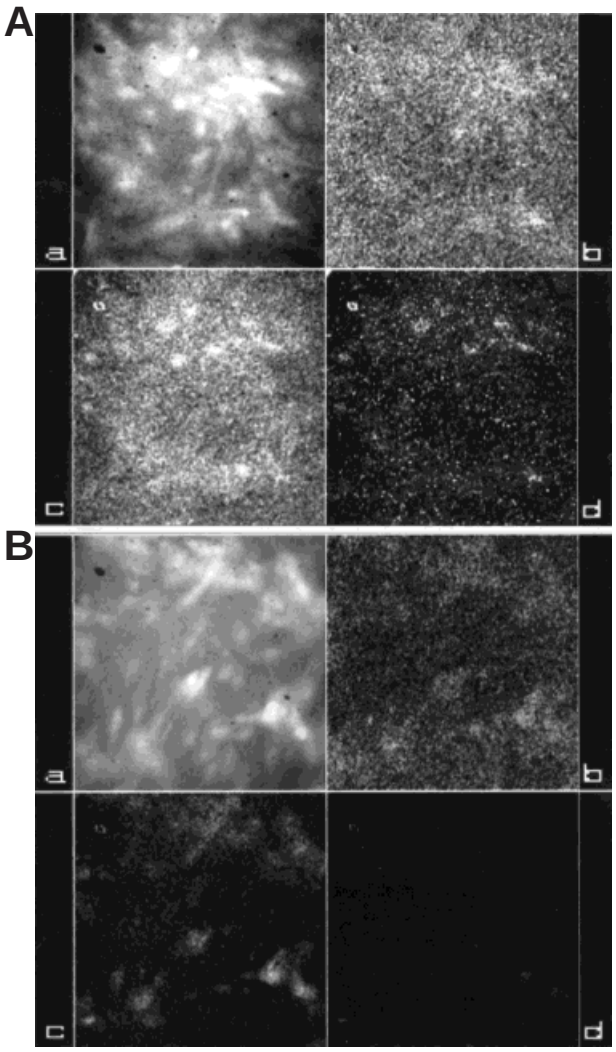

FIG. 10. Examples of parametric images obtained after modeling by an analytical model (here: the three-parameter model: $I_n = \alpha(0) + \alpha(1) \cdot [1 - \exp(-\alpha(2) \cdot n])$. a–c: Parametric images: $\alpha(0)$, $\alpha(1)$, and $\alpha(2)$. d: Chi-square. **A:** Results computed from Figure 1A. **B:** Results computed from Figure 1B.

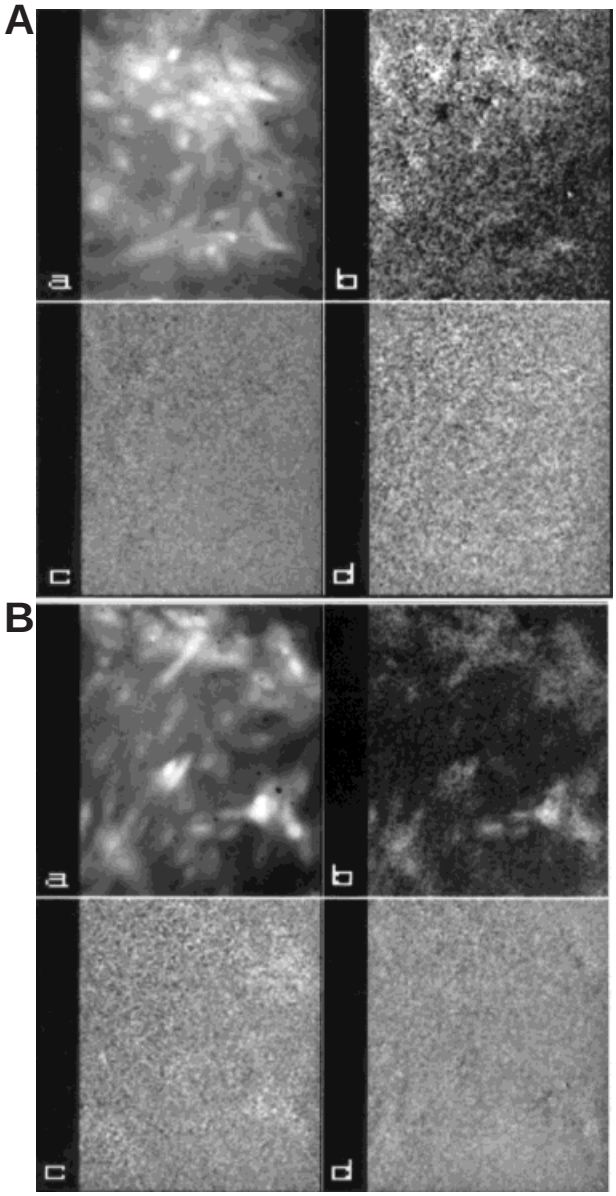

FIG. 11. Factorial images resulting from the application of multivariate statistical analysis (in fact, principal components analysis) to the experimental series of Figure 1. a: The ''trivial'' factorial image is the average of the 15 experimental images. b: This factorial image, corresponding to axis 1, contains most of the information relevant to the temporal behavior. c: This factorial image, corresponding to axis 2, contains the residue of the information. d: The factorial image corresponding to axis 3 contains only noise. **A:** Results computed from Figure 1A. **B:** Results computed from Figure 1B.

ated cells (7). The methods investigated in the present work are of interest in order to analyze the abnormal functional expression of the CFTR protein, which may not only be caused by CFTR gene mutations, but can also be associated with airway surface epithelium dedifferentiation and remodeling.

It appears that two types of methodology are available for extracting qualitative and quantitative information from fluorescence videomicroscopy, i.e., from sequences of fluorescence images recorded as a function of time.

In the first methodology, the different intensity values at one pixel site (or the average of intensity values within a region of interest, a cell, for instance) are combined with a model of the intensity variation in order to get one (or a few) quantitative parameter(s) describing the behavior of this pixel or ROI. When this procedure is repeated for every pixel, new (synthesized) images can be obtained (parametric images). These new images can be displayed, processed (segmented into different regions for instance) and analyzed in order to obtain a global result for the whole field of view. The statistical significance of the results is improved when this procedure is applied to ROIs. However, the main drawback of the modeling approach remains, i.e., which model should be used? Moreover, it is difficult to compare the results of modeling obtained for different objects, because a model (especially

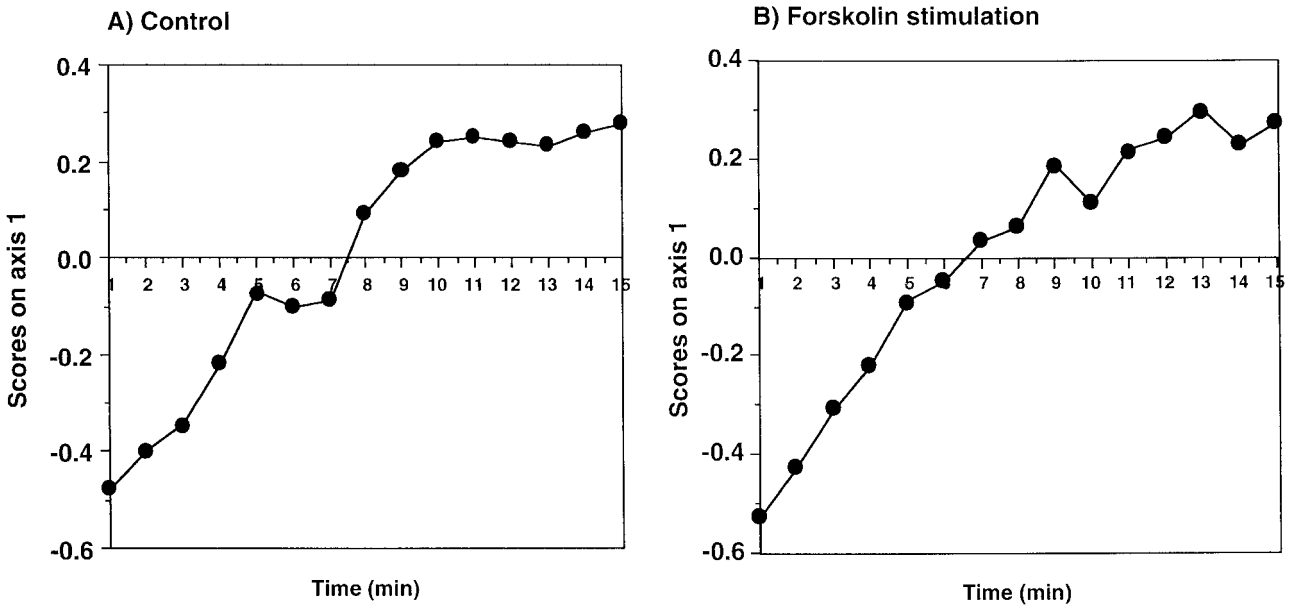

FIG. 12. First factorial curve (corresponding to factorial axis 1), resulting from the application of principal component analysis. This curve displays the overall shape of the model that describes the temporal behavior. **A:** Results computed from Figure 1A. **B:** Results computed from Figure 1B.

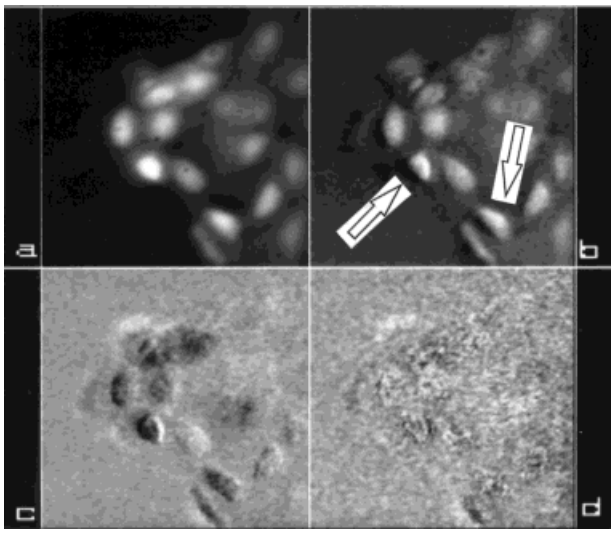

FIG. 13. Illustration of the need to interpret the results of MSA carefully. Here, the four factorial images **(a–d)** obtained after analyzing the series of Figure 2 are displayed. The factorial image corresponding to axis 1 (b) displays a strong contrast for the left part and the right part of some cells. This contrast is mainly due to a displacement of these cells during the experiment, and not to a variation of the fluorescence intensity.

an analytical model) cannot generally be described by a single parameter.

Alternatively, the whole image sequence can be analyzed at once by multivariate statistical methods. In this case, the factorial images permit the visualization of different ''sources of information'' present in the dataset, without the need to choose a model to describe the temporal evolution. Moreover, the underlying models are provided by the analysis itself, within the limits that the original data be considered as the linear combination of several orthogonal components.

However, this interesting ability of MSA to analyze the whole dataset at once is also its weakness. Since the whole image is considered, results can be obscured, or even completely disturbed, by some ''imperfections'' (or artifacts) of the experimental data. Suppose for instance that we are studying weak temporal fluorescence variations in stationary cells (let us recall that, in this paper, we are not considering the problem of moving objects). Now, if one or several cells move during the image sequence acquisition, the main source of information (i.e., of intensity variance) that will be detected is the cell movement, and the useful information (fluorescence variation) will be obscured by this artifact. This problem was illustrated in Figure 13.

Thus, one must be very careful when using results obtained by MSA. Only those results that can be interpreted (in terms of factorial images and factorial curves) as being almost free of artifacts can be significant. On the other hand, we can say that this ability of MSA to display the different sources of information (including experimental artifacts) can be considered as an important property of MSA, compared to other methods in which the quantitative results are obtained blindly, i.e., without the opportunity to visualize and interpret intermediate results.

Finally, it is difficult to make a definitive choice between the two types of approaches: the modeling approach and the multivariate analysis approach. We suggest the following:

1. Apply MSA in order to get a rough idea of the content of the experimental series, in terms of number of sources

of information (number of high eigenvalues), of spatial contrast (factorial images), and of temporal models (factorial curves). At this stage, experimental artifacts can be detected and eventually be compensated for (a drift of the microscope stage or of the specimen, for instance, can be corrected).

2. If one of the ''factors'' obtained during the decomposition can be identified (after interpretation) as the phenomenon one wants to analyze, quantification can be done within the framework of MSA.

3. MSA can also be considered as a prescreening technique allowing for the detection of artifacts and/or the visualization of the type of underlying model, which aids in the choice of an analytical model. The factorial images (and especially the first one) can also be used to segment the field of view into homogeneous regions of interest, i.e., into zones with a similar temporal behavior. When this is done, it is then possible to return to modeling techniques in order to obtain quantitative results in terms of the model parameters, for the different regions of interest.

In conclusion, the use of the former strategy should result in new approach to precisely analyze physiological parameters within a cell population or in different compartments within a cell.

ACKNOWLEDGMENTS

We thank Professor J.M. Klossek (Hôpital Jean Bernard, Poitiers, France) and Dr. X. Hannion (Polyclinique Courlancy, Reims, France) for providing human airway tissue, together with D. Pierrot for his expertise in cell culture and H. Kaplan for setting up the digital image acquisition procedure.

We thank the anonymous referees and the Associate Editor of the journal for their helpful comments on the first version of the manuscript, enabling us to improve it significantly.

LITERATURE CITED

1. Benzecri JP: L'analyse des données. Dunod, Paris, 1978.
2. Bevington PR: Data Reduction and Error Analysis for the Physical Sciences. McGraw-Hill, New York, 1969.
3. Bonnet N, Simova E, Lebonvallet S, Kaplan H: New applications of Multivariate Statistical Analysis in microscopy and spectroscopy. Ultramicroscopy 40:1–11, 1992.
4. Bonnet N, Trebbia P: Multi-dimensional data analysis and processing in electron-induced microanalysis. Scann Microsc 6 (suppl):163–177, 1992.
5. Bonnet N: Preliminary investigation of two methods for the automatic handling of multivariate microanalytical maps. Ultramicroscopy 57:17–27, 1995.
6. Brakenhoff GJ, Visscher K, Gijsbers EJ: Fluorescence bleach rate imaging. J Microsc 175:154–161, 1994.
7. Brezillon S, Dupuit F, Hinnrasky J, Marchand V, Kälin N, Tûmmler B, Puchelle E: Decreased expression of the CFTR protein in remodeled human nasal epithelium from noncystic fibrosis patients. Lab Invest 72:191–200, 1995.
8. Chevillard M, Hinnrasky J, Zahm JM, Plotkowsky C, Puchelle E: Proliferation, differentiation and ciliary beating of human ciliated cells in primary culture. Cell Tissue Res 264:49–55, 1991.
9. Dantzig GB: Linear Programming and Extensions. Princeton University Press, Princeton, NJ, 1963.
10. Di Paola R, Bazin JP, Aubry F, Aurengo A, Cavailloles F, Herry A, Kahn E: IEEE Trans Nucl Sci 29:1310, 1989.
11. Esbensen KH, Geladi PL, Grahn HF: Strategies for multivariate image regression. Chem Int Lab Syst 14:357–374, 1992.
12. Gill PE, Murray W, Wright MH: Practical Optimization. Academic Press, San Diego, 1981.
13. Goldberg DE: Genetic Algorithms in Search, Optimization and Machine Learning. Addison-Wesley, Reading, 1989.
14. Grahn H, Szeverenyi NM, Roggenbuck MW, Geladi P: Tissue discrimination in magnetic resonance imaging: A predictive multivariate approach. Chem Intell Lab Syst 7:87–93, 1989.
15. Herbin M, Bonnet N, Vautrot P: A clustering technique based on the estimation of the probability density function and on the skeleton by influence zones. Application to image processing. Patt Rec Lett 17:1141–1150, 1996.
16. Himmelblau D: Applied Nonlinear Programming. McGraw Hill, New York, 1972.
17. Huang TS (ed): Image Sequence Analysis. Springer-Verlag, Berlin, 1981.
18. Inoue S: Video-microscopy. Plenum Press, New York, 1987.
19. Jovin TM, Arndt-Jovin DJ, Marriott G, Clegg RM, Robert-Nicoud M, Schormann T: Distance, wavelength and time: The versatile 3rd dimensions in light emission microscopy. In: Optical Microscopy for Biology, Herman B, Jacobson K (eds). Wiley-Liss, New York, 1990, pp 575–602.
20. Kahn E, Hotmar J, Frouin F, Di Paola M, Bazin J-P, Di Paola R, Bernheim A: Spectral and dynamic confocal fluorescence characterization of cytogenetic preparations. Anal Cell Pathol 12:45–56, 1996.
21. Kirkpatrick S, Gelatt C, Vecchi M: Optimization by simulated annealing. Science 220:671–680, 1983.
22. Lebart L, Morineau A, Warwick KM: Multivariate Descriptive Statistical Analysis. John Wiley & Sons, New York, 1984.
23. Liehn JC: Synthèse et analyse des images paramétriques en médecine nucléaire: analyse d'ensembles d'images par la méthode du modèle. Thesis, Université de Reims, France, 1988.
24. Liehn JC, Hannequin P, Valeyre J: L'analyse des séquences d'images en Médecine Nucléaire. 1. Application de la méthode du modèle à l'imagerie paramétrique. J Med Nucl Biophys 13:61–77, 1989.
25. Malinowski E, Howery D: Factor Analysis in Chemistry. Wiley-Interscience, New York, 1980.
26. Moik JG: Digital Processing of Remotely Sensed Images. NASA Scientific and Technical Information Branch, Washington, DC, 1980.
27. Richalet J, Rault A, Pouliquen R: Identification des processus par la méthode du modèle. Gordon & Breach, Paris, 1971.
28. Soltanian-Zadeh H, Windham JP, Peck DJ, Yagle AE: A comparative analysis of several transformations for enhancement and segmentation of magnetic resonance scene sequence. IEEE Trans Med Imag 11:302–318, 1992.
29. Trebbia P, Bonnet N: EELS elemental mapping with unconventional methods. I. Theoretical basis: Image analysis with multivariate statistics and entropy concepts. Ultramicroscopy 34:165–178, 1990.
30. Van Heel M, Frank J: Use of multivariate statistics in analysing the images of biological macromolecules. Ultramicroscopy 6:187–194, 1981.
31. Vigo J, Salmon JM, Lahmy S, Vialley P: Fluorescent image cytometry: from qualitative to quantitative measurements. Anal Cell Pathol 3:145–165, 1991.
32. Weiss D, Maile W, Wick RA: Video microscopy. In: Light Microscopy in Biology: A Practical Approach, Lacey AJ (ed). Oxford University Press, Oxford, 1989, pp 221–278.
33. Windham JP, Abd-Allah MA, Reimann DA, Froehlich JW, Haggar AM: Eigenimage filtering in MR imaging. J Comput Assist Tomogr 12:1–9, 1988.
34. Zahm JM, Bonnet N, Pierrot D, Dupuit F, Puchelle E: Airway cAMP-activated chloride efflux is preferentially expressed in ciliated cells. Pediatr Pulmonol 512:194–195, 1995.